Electronic Supplementary Material (ESI) for Journal of Materials Chemistry C.
This journal is © The Royal Society of Chemistry 2014

Reducing the effects of shot noise using nanoparticles

Moshood K. Morakinyo[b] and Shankar B. Rananavare[a1]

MATERIALS AND METHODS

Chemicals. The following chemicals were used without further purification: Gold colloids (Ted Pella Inc.); hydrogen peroxide, hydrochloric acid, ammonium hydroxide, hydrogen fluoride (Fisher Scientific); toluene (anhydrous, 99.8 %), isopropyl alcohol (IPA), methyl butyl ketone (MIBK), 1:3 MIBK:IPA developer, 950 k poly(methyl methacylate (PMMA, 4 % in Anisole), (Sigma-Aldrich); N-(2-aminoethyl)-11-aminoundecyltrimethoxysilane (AATMS, > 95 %, Gelest Inc.). Doubly-distilled and deionized water (Barnstead Sybron Corporation water purification Unit, resistivity of 19.0 MΩcm) was used for cleaning apparatus and for washing substrates.

Methods.

Derivatization and characterization. Positively charged Self-Assembled Monolayers (SAMs) of aminosilane were formed on the surface of silicon oxide wafers by incubating the samples in 0.05 M solution of AATMS, prepared in dry toluene at 80 °C for 15 minutes, sonicated in pure toluene for 2 minutes and then dried in a stream of nitrogen gas. AATMS film thickness was measured by Gaertner ellipsometer (He-Ne laser light source, λ = 632.8 nm, fixed incidence angle of 70°). Surface elemental compositions were characterized by x-ray photoelectron spectroscopy (XPS, ThermoScientifc ESCALAB 250 instrument).

E-beam patterning. Aminosilane derivatized wafers were spin coated (4000 rpm) with PMMA resist, pre-baked at 180 ˚C for 120 s, patterned using e-beam (Zeiss sigma VP FEG SEM), developed in 1:3 MIBK:IPA developer for 70 s, washed in IPA for 30 s and in water for 30 s, and then dried in a stream of nitrogen gas to produce 80 - 100 nm contact holes. The e-beam parameters are 10 microns aperture, 30 kV accelerating voltage, 37 pA beam current, 160 nm pitch and a dose of 24 μC.

Gold nanoparticle deposition. Gold nanoparticles (GNPs) deposition was achieved by the immersion of pre-patterned wafers in GNPs solutions at room temperature. The bulk deposition process could handle different size substrates and/or more than one substrate at a time. Duration of deposition varied from few hours to 1 day depends on NP sizes and hole diameters. After deposition samples were washed with deionized water and then dried in a stream of nitrogen gas. In the deposition studies, loosely bound nanoparticles on the resist surface were observed but not in nano-wells. Two minutes of low-power ultra-sonication removed these aggregates deposited on the resist surface, leaving only the strongly bound nanoparticles in the nanoholes. Loading, or

[1] Author for correspondence, ranavas@pdx.edu. [a] SBR is at the Department of Chemistry, Portland State University, Portland, OR 97206. Currently, [b] MKM is at Portland Technology Development Labs at Intel Corporation, Ronler Acres Hillsboro OR 97124.

multiple particle deposition, effects were more significant when the deposition was conducted from a solution containing higher concentration of nanoparticles.

Scanning electron microscopy imaging. An FEI Siron XL30 model SEM was used for electron microscopy imaging. Imaging was performed at an accelerating voltage of 5 kV at beam current of ~300 μA.

Pattern formation. The first step is a *resist reflow process* (RRP) in which PMMA was made to reflow at a pre-determined flow rate of 1.67 ± 0.14 nm/s into the contact holes, containing the deposited GNPs of the desired pattern sizes. This was achieved by baking PMMA resist at a temperature (100 ˚C) slightly below its pre-determined glass transition temperature (110 ± 1.0 ˚C). Following RRP is *dry etching* where oxygen plasma was used to reduce the thickness of PMMA to 10 nm, the radius of the GNPs. The final step in pattern formation is *iodine etching* of GNPs using 0.1 M iodine solution (5% I_2 + 10 % KI + 85 % H_2O) to produce contact holes of the same dimensions as the GNPs.

Cost of implementation. Given the preliminary nature of these results, only a qualitative discussion of implementation costs of the method in a VLSI/CMOS process flow is presented below.

a. The cost of nanoparticles is high since these are gold nanoparticles and the nanoparticle size is controlled by successive separation. However, the gold NPs could be replaced with cheaper silica nanoparticles which would reduce the cost.
b. Thermal annealing step employed in resist reflow would be comparable in cost to the prebaking/postbaking steps commonly employed in the standard lithographic processing. Therefore this step could be carried out on similar equipment.
c. The costs for O_2 plasma etching of the resist would be comparable to oxygen ashing.
d. The wet etching of nanoparticles would be inexpensive as it does not use any exotic chemistry, only relying on inexpensive HF (for silica particles) and Iodine/KI mixture (for gold nanoparticles).
e. The main cost would be in the deposition process as it would take at least few hours; however as discussed before, multiple wafers in a single deposition bath allows parallel processing.

Thus, the method does not require creation of new tools for its implementation. Our conjecture is that the overall costs would be comparable to, or lower than, the conventional multiple patterning.

Figure S1: Molecular Structure of AATMS. At the pH employed during nanoparticle deposition both amine groups are expected to acquire positive charge as typical values of pKa for primary (secondary) amines are above 9 (7.5). [2, 3]

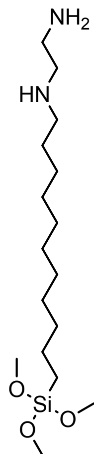

N-(2-AMINOETHYL)-11-AMINOUNDECYLTRIMETHOXYSILANE

Equation S1 A simple steric model to calculate nanoparticle packing density on the surface

Assuming random loose packing of gold NP on the derivatized surface, it is easy to show that the packing density on the surface is given by:

$$S = \frac{\alpha}{(2a + \beta l_D)^2}$$

S = particle density

a = Particle radius

l_D = Debye length

$\propto \frac{1}{\sqrt{I}}$ I = ionic strength

α, β : adjustable parameters.

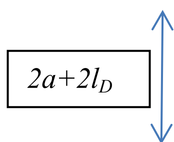

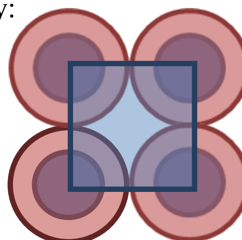

β= 2 for the closest square planar packing as shown to the right. For the fit shown figure 1 we let α and β vary as free parameter to account for loose packing on the surface.

Table S1 Particle density distribution and related quantities for deposition on AATMS-SAM derivatized and unpatterned wafers

Au NP diameter, 2a (nm)	conc ×10^9 (Particles/mL)	Average particle density *S(particles//μm²)*	*Area ratio* $S*4\pi a^2/1\mu m^2$	mean particle separation (nm) $P^U = 10^3/\sqrt{S}$	$P^U/2a$
10	5700	2219 ± 53	0.70	21	2.1
15	1400	1243 ± 78	0.88	28	1.9
20	700	636 ± 67	0.80	40	2.0
30	200	336 ± 34	0.95	55	1.8
40	90	188 ± 5	0.94	73	1.8
50	45	111 ± 18	0.87	95	1.9
60	26	83 ± 5	0.94	110	1.8
100	5.6	9 ± 3	0.29	330	3.3

Table S2. Effect of ionic strength on particle deposition, Au NP (20 nm diameter) concentration 5.86 × 10^{11} particles/mL, AATMS film thickness 4 nm, Deposition time 240 minutes. It indicates higher ionic strength leads to higher packing density due to reduction in Debye (ionic screening) length

ionic strength	Debye length l_d (nm)	Particle density $S(N/\mu m^2)$	Mean particle separation (nm) $P^U = 10^3/\sqrt{S}$	$P^U/2a$
NP solution (resuspended in DI water)	25	400	50	2.5
pH 7	4	625	40	2
pH 7 + 8 mM NaCl	2	730	37	1.8

Table S3. The particle density on surface depends on the pH of depositing solution

pH	Debye Length l_d (nm)	Particle density $S(N/\mu m^2)$	Mean Particle separation (nm) $P^U = 10^3/\sqrt{S}$	$P^U/2a$
4.5	7.1	577	42	2.1
5	6	566	42	2.1
5.5	5.3	603	41	2.1
6	4.8	629	40	2.0
6.5	4.3	664	39	1.95
7	4.1	694	37	1.85

Figure S2 Effect of ionic strength on particle density, and mean separation between particles. The change in ionic strength affects the Debye length which in turn controls the packing density according to the equation given in IV above.

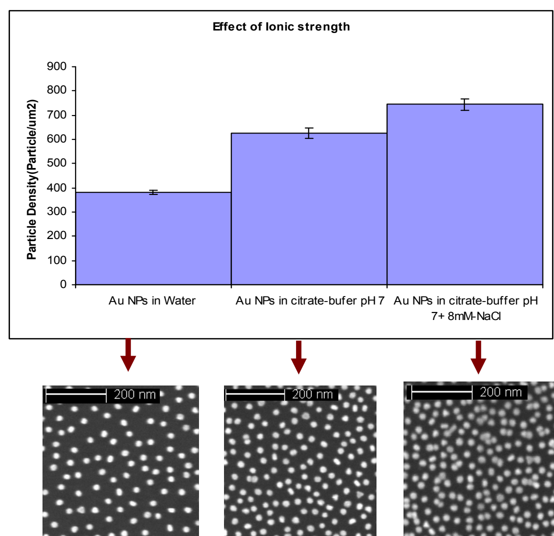

Figure S3 Effect of pH on particle deposition. Below pH 4 nanoparticles begin to coagulate and precipitate out of solution. Particle density appears to follow simple behavior given in Figure 1 with $\beta = 0.7 \pm 0.1$ and $\alpha = 1.1 \pm 0.6 \times 10^5$. This fitted curve (green line) is shown in the inset shown below.

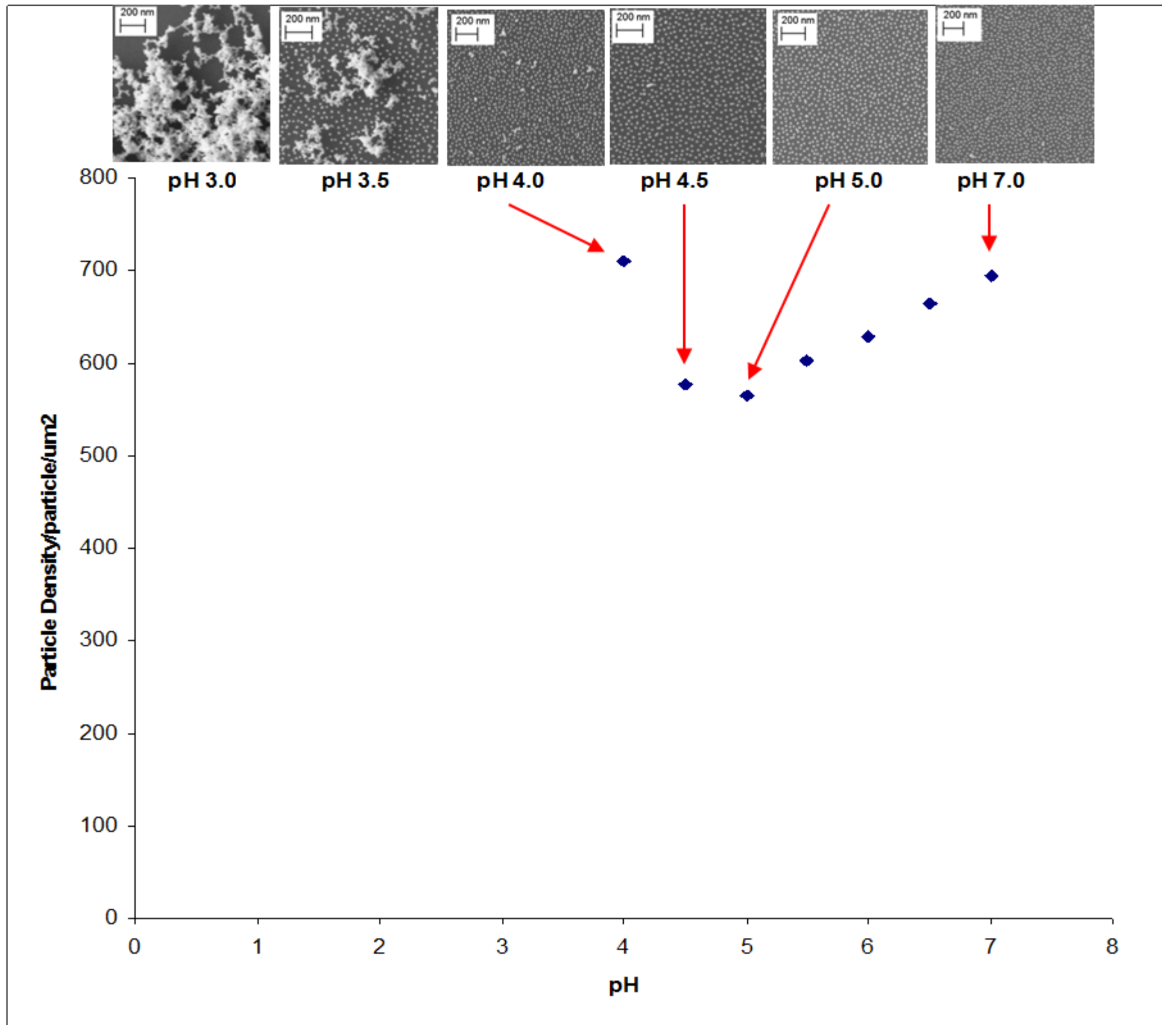

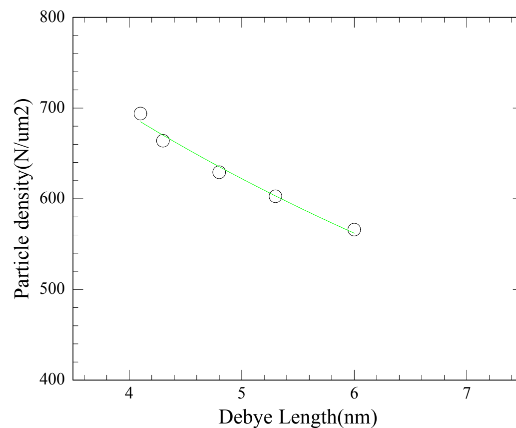

Figure S4 The equilbrium area ratio (total area of nanoparticles deposited/μm^2 area of substrtate, 4th column Table S1) is independent of particle size(shown) or concentration (not shown). The error bars were evaluated from the three times the standard deviations in the avarage particle densisty σ given in the Table S1. Linear fit gave slope of 0.003 ± 0.002 and intercept of 0.76 ± 0.06 and zeroth order fit gave the draw red line with intercept of 0.87 ± 0.09. Thus, within experimental errors the slope is zero.

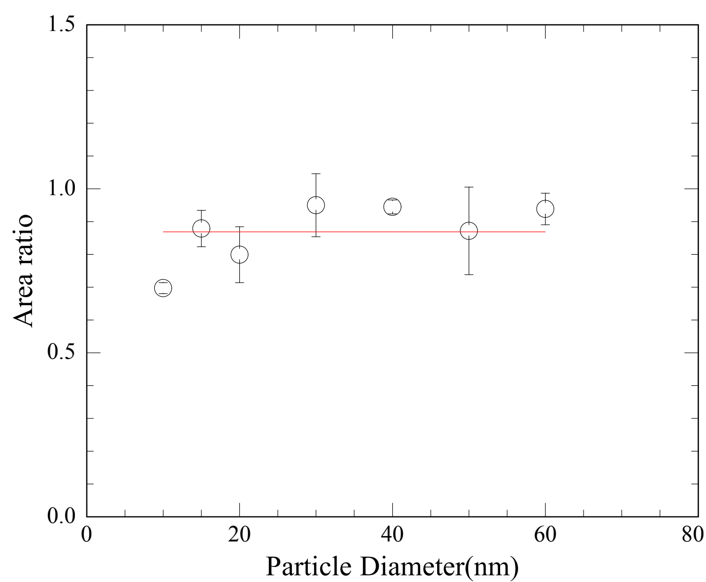

Table S3 Filling fractions and average number of particles per hole. Pitch is fixed at 200 nms. The average number of particles deposited is a function of time. The data presented below employed fixed duration of 24 hours and fixed concentration of nanoparticles.

Hole diameter (nm)	fill fraction (exp)	avg#/hole (exp)	Poisson eqn.(pred)	Fill fraction (exp)	avg#/hole (exp)	Poisson eqn.(pred)	Fill fraction (exp)	avg#/hole (exp)	Poisson eqn(pred)
	10 nm (AuNP)			15 nm (AuNP)			20 nm (AuNP		
30	0	0	0	0	0.15	0.14			
40	0.29	0.29	0.25	0.54	0.6	0.45	0	0	0
50	0.64	0.57	0.43	0.92	1.5	0.78	0.5	0.58	0.44
60	0.76	0.88	0.59	0.96	2.8	0.86	0.97	2.22	0.89
70				0.99	4.7	0.94	0.98		0.93
80							0.99	2.88	0.94
90							0.99		

These studies preliminary provide guidance for future optimization of deposition process that would involve variation of ionic strength, pH of the depositing solution as well as variation in charge density in resist polymer, SAM. The overall goal here is to improve fill fractions and though electrostatic/surface interactions.

Figure S5 Fill fraction obeys Poisson statistics. The average number of particle per hole, <*N*> can be used to calculate fraction of holes filled. The symbols in figure below are experimental points and the lines are calculated values by measuring the average number of particles per hole determined from SEM images.

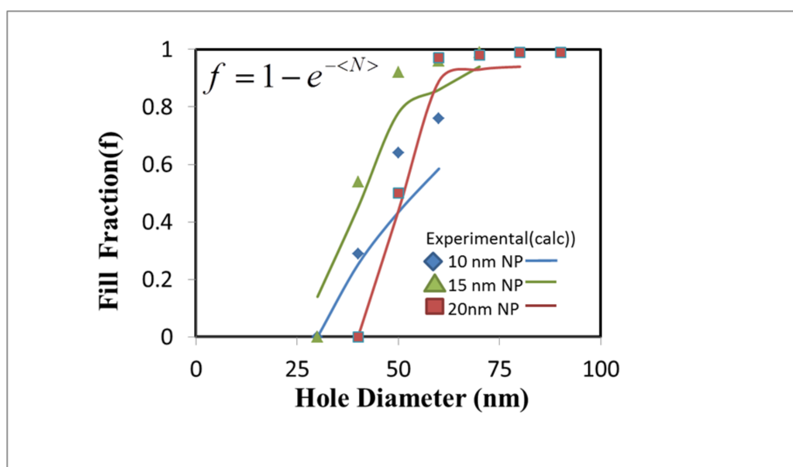

It should be noted that in these studies the ionic strength of the nanoparticle dispersion varies. We believe the extraporlated limiting hole size (≈ 25nm) can be reduced by changing surface charge densities of the PMMA and SAM exposed to the depositing solution (see below).

Figure S6 Typical pitch needed for planar transistors based on (http://www.itrs.net/Links/2012ITRS/2012Chapters/2012Overview.pdf

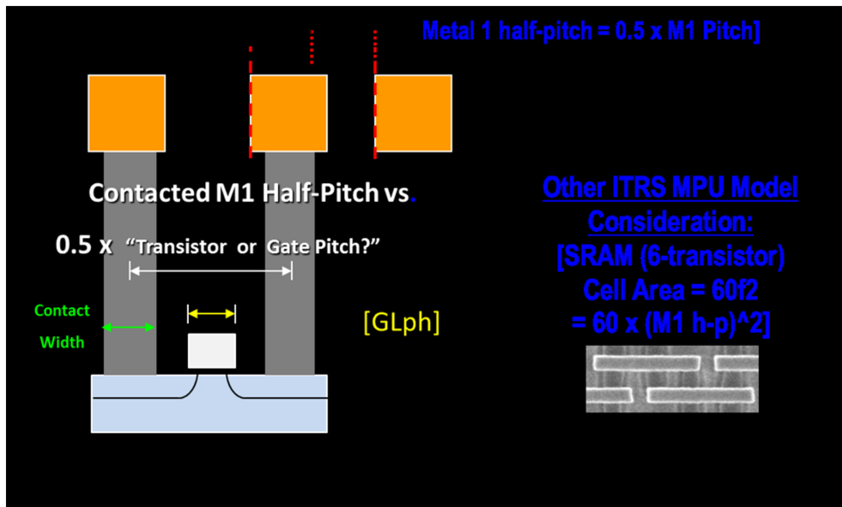

Spacing between the centers of metal lines connecting to source and drain regions of transistors should meet:

$P_{transistor}$>gate length+contact width

$P_{transistor}$ >gate length+D.

Based on these consideration the proposed via fabrication scheme would potentially enable 5nm gate length.

General limitations and methods to improve the approach

(1) Improved nanoparticle centerning in holes:

As can be gleaned from the FFTs presented in Figure 4 the positional misplacment degrades the registry of the fabricated holes. This results from Gaussian positional distribution with respect to the center of hole as shown in Figure 7. Electrostatic funneling potential and the corresponding force, in the Classical Derjaguin Limit(CDL), that drives the nanoparticle to the hole center, are given as [1]:

$$U(r)=\frac{4\pi a\varepsilon\psi_0^2}{\sqrt{1-2a/D}}\left\{\begin{array}{l}\ln(\exp([D/2-a-r]/l_d)+1))-\ln(\exp([D/2-a+r]/l_d)+1)\\ -\gamma_0 l_D\left(\dfrac{1}{([D/2-a-r]/l_d)}-\dfrac{1}{([D/2-a+r]/l_d)}\right)\end{array}\right\}$$

$$F(r)=\frac{4\pi a\varepsilon\psi_0^2}{l_d\sqrt{1-2a/D}}\left\{\begin{array}{l}\dfrac{1}{\exp([D/2-a-r]/l_d)+1}-\dfrac{1}{\exp([D/2-a+r]/l_d)+1}\\ -\gamma_0 l_D\left(\dfrac{1}{([D/2-a-r]/l_d)^2}-\dfrac{1}{([D/2-a+r]/l_d)^2}\right)\end{array}\right\}$$

$\psi_0 = surface\ potential\ of\ membrane\ and\ GNP,\ \varepsilon\ dielectric\ cons\tan t,\ l_d\ Debye\, length$

$$\gamma_0=\frac{A}{24\pi\varepsilon l_d\psi_0^2}$$

$Where\ A\ is\ Hama\ker\ const.\ Here\ we\ set\ \psi_{Membrane}=\psi_{Particle}=\psi_0$

The corresponding geometric parameters are defined in the figure below:

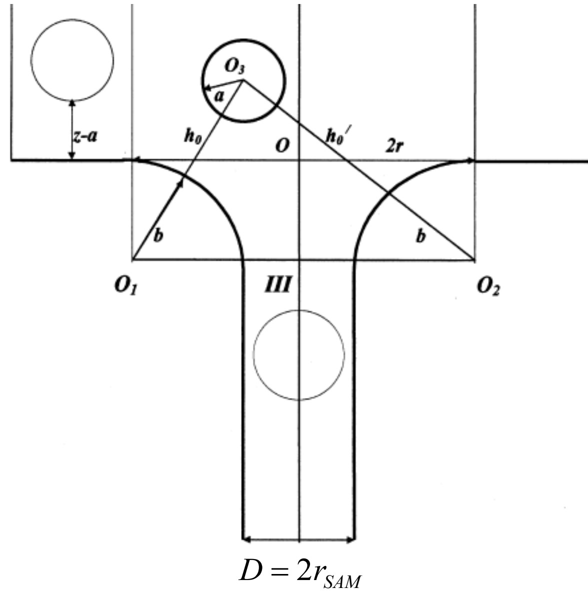

Figure S7 Scheme of interaction of a spherical particle with a membrane pore: a, radius of the particle; b, radius of the rounding of the pore entrance; r_{SAM} , radius of the membrane pore; (Figure adapted from [1]).

Therefore, higher values of F are realized by (1) making $2a \approx D$; note for the results presented in Figure 4, $2a/D = 0.25$. (2) Increasing the ionic strength; this reduces the value of Debye length; experiments in Figure 4, employed $l_d \approx 4.0\ nm$. (3) Increasing zeta potentials on surfaces through increased surface charge densities.

The experimental data in Figure 3 b, bottom right was fitted to a simple weighted potential as follows:

$$Particle\ Density(r) = \exp(-U(r)/k_B T$$

Where $U(r)$ is defined above. Remarkably by varying just two parameters l_d and γ_0 the data can be well fitted to extract the values of these two parameters. Knowing values the charge densities (see main text) it is possible to relate them to different surface potentials of GNP and PMMA using equations given elsewhere [4] to further improve the $U(r)$. As data in figure below can also be readily fitted to simple Gaussian with insignificant difference in χ^2, adding these additional parameters in the equation was considered over parameterization.

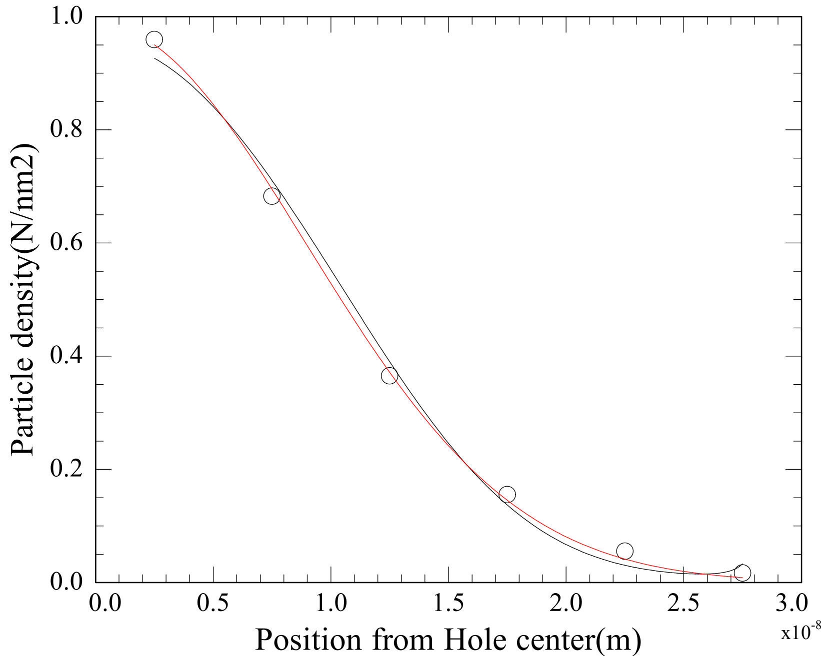

Figure S8: Particle density was determined from positional distribution of NP centers from the center of about 500 holes. Nonlinear least squares data analysis for CDL model was used to fit the ratio of Hamaker/electrostatic contributions $\gamma_0 = 0.10 \pm 0.01$, and the Debye length $l_d = 8.5 \pm 0.4$ nm; while keeping the following parameters fixed: $k_B T = 4.114\times10^{-21}$ J, Medium dielectric constant $\varepsilon_{Water} = 80$, $\psi_{PMMA} = \psi_{GNP} = 25$mV.,$D = 80$ nm, $2a = 20$ nm, Fitting data to simple Gaussian is shown as a red curve with the best fit value of $\sigma = 9.0 \pm 0.1$nm.

(2) Estimating and reducing r^{C}_{SAM} :

A. There exists a repulsive potential barrier for negatively charged GNP particle entering the pore, of diameter D and radius of curvature b, in a negatively charged resitst film of PMMA. The normalized axial potential experienced by a particle of radius, a, near the pore entry varies[1] as:

$$\breve{U}(z) = \frac{2(a/l_d)\psi_m^2}{\sqrt{\left(1+\frac{a}{b}\right)\left(1-\frac{2a/D}{1+2b/D}\right)}} \times \left(\left(1+\frac{\psi_p}{\psi_m}\right)^2 \ln(1+\exp(-\xi)) + \left(1-\frac{\psi_p}{\psi_m}\right)^2 \ln(1-\exp(-\xi)) - \frac{\gamma_m}{\xi} \right)$$

$$\xi = 2a/D\sqrt{\left(\frac{1+2b/D}{2a/D}\right)^2 + \left(\frac{b+z}{a}\right)} - \frac{b}{a} - 1$$

$$b = radius\ of\ curvature\ at\ pore\ opening\ in\ x-z\ plane$$

Please note in the above equation, z refers to the vertical translation along the center of the pore, and not the PMMA resist thickness. The location z= 0 corresponds to the particle center of mass at the pore opening. The repulsive potential for nanoparticle entry must be overcome by the attractive electrostatic potential provided by the oppositely charged AATMS SAM at the bottom of the pore. Thus, strategies to reduce critical pore size, r^{C}_{SAM}, would require (1) increasing the charge density (surface zeta potential) at the bottom of hole by increasing the positive charge on the molecular structures forming SAM; (2) decreasing b to reduce the height of the barrier. This is analogous to decreasing pitch P as discussed before in the main text (see below).

B. A simple charge balance model to estimate r^{C}_{SAM}:

$$\rho_{SAM}\pi r_{SAM}^2 - \rho_{PMMA}(2\pi r_{SAM} z + P^2 - \pi r_{SAM}^2) = 0$$

$$r_{SAM} = D/2$$

$$r_{SAM}^C = \frac{\rho_{PMMA}\, z}{\rho_{PMMA} + \rho_{SAM}}\left(1+\sqrt{1+\theta}\right)$$

$$\theta = \frac{P^2(\rho_{PMMA} + \rho_{SAM})}{\pi\rho_{PMMA} z^2}$$

$$r_{SAM}^C = \frac{\rho_{PMMA}\, z}{\rho_{PMMA} + \rho_{SAM}} \quad \theta << 1 \qquad r_{SAM}^C = \sqrt{\frac{\rho_{PMMA}}{\pi(\rho_{PMMA} + \rho_{SAM})}}P \quad \theta >> 1$$

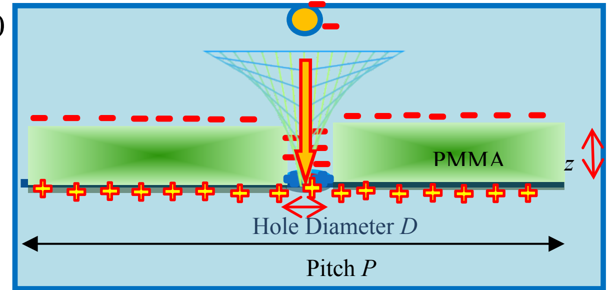

Here ρ_i's are the effective charge densities on solution exposed surfaces of wafer (i.e., the exposed hole bottom, ρ_{SAM} and PMMA resist, ρ_{PMMA}). Here z and r_{SAM} are the thickness of the resist film and radius of the holes in the photoresist film, respectively. Both classic Derjaguin approach as well as simple electrostatic approaches provides us with consistent guidance in improving the method.

(3) Chemically altering spatial reactivity in the patterned holes :

Another solution to centering would be to exploit the spatial intensity distribution (highest at the center) of the beam to create more reactive species at the center of nanohole. This could be achieved by using photo-labile pendant groups containing SAMs that decompose upon exposure to the radiation. Amine-based photobase generators are known[5] and could be adapted to provide reactive center (positively charged) and not so reactive outer edge of the nanohole.

Given the large parameter space, optimization of the deposition process is nontrivial and our ongoing studies attempt to improve the method.

Bibliography

1. W. Richard Bowen, A. N. Filippov, A. O. Sharif and V. M. Starov, *Advances in Colloid and Interface Science*, 1999, **81**, 35-72.
2. V. S. Bryantsev, M. S. Diallo and W. A. Goddard, *The Journal of Physical Chemistry A*, 2007, **111**, 4422-4430.
3. H. Zhang, H.-X. He, T. Mu and Z.-F. Liu, *Thin Solid Films*, 1998, **327(329)**, 778-780.
4. K. Kimura, S. Takashima and H. Ohshima, *The Journal of Physical Chemistry B*, 2002, **106**, 7260-7266.
5. G. L. Hallett-Tapley, T.-L. Wee, H. Tran, S. B. Rananavare, J. M. Blackwell and J. C. Scaiano, *Journal of Materials Chemistry C*, 2013, **1**, 2657-2665.